

Digital Image Correlation: A Measurement Tool For the Study of Explosive Effects

Mark W. Nansteel
Battelle Memorial Institute
Transportation Security Laboratory
William J. Hughes Technical Center
Atlantic City International Airport, NJ 08405
(609) 813-2821
Mark.Nansteel@associates.dhs.gov

Charles Chih-Tsai Chen
DHS/S&T/TSL-120
Transportation Security Laboratory
William J. Hughes Technical Center
Atlantic City International Airport, NJ 08405
(609) 813-2814
Chih-Tsai.Chen@dhs.gov

Abstract—*It is difficult to measure the response of a structure to an explosive blast because of the high speed and transient nature of the deformation and also the severity of shock effects. Measurement approaches using strain gages and accelerometers provide point-wise information only and may be adversely influenced by shock-related noise. Further, attached sensors of even small mass can separate from the structure or subtly perturb the local response of lightweight structures. Global or full-field capability is especially important owing to the unpredictable spatial response characteristics. High speed photography in combination with digital image correlation allows full-field, non-intrusive measurements of the high speed dynamic response of structures to blast forces. Image correlation measurements yield transverse and in-plane surface displacement and surface strains. High speed photography and digital image correlation are used to study the elastic and plastic response of flat and curved aluminum panels and planar witness plates to blast forces.*

1. INTRODUCTION

Because of the ever present potential for terrorist attack using explosives it is important to evaluate the vulnerability of structures to blast forces. In some cases it may also be possible to develop strategies for mitigating blast structural damage and catastrophic failure. The most important component of vulnerability assessment or mitigation development is the ability to either predict or measure the response of a structure to a particular blast load. This is particularly difficult in the case of lightweight aircraft structures. In addition to the challenges posed by the highly transient nature of the response there may be only one opportunity to gather useful data if the structure under test is damaged or destroyed. This means that optimal placement

of sensors such as strain gages and accelerometers on the structure is critical if key data is to be collected from a single test. This is especially demanding owing to the point-wise nature of the information available from these sensors and the rather unpredictable spatial response characteristics. Further, attached sensors of even small mass can separate from the structure or they can subtly perturb the local response of lightweight aircraft structures when shock-induced accelerations are high.

A full-field non-contact measurement technique greatly increases the probability that data will be captured in critical areas of the structure without distortion of the desired test conditions. A market survey of full-field non contact methods was conducted at the Transportation Security Laboratory (TSL) at the W. J. Hughes Technical Center in the fall of 2005. Holographic and speckle pattern interferometry and digital image correlation were considered in the survey, however, it was found that only digital image correlation is capable of resolving the large displacements which typically result during blast-induced deformation of aircraft structures. Development of this technology began in the 1980's [1-2] but it only evolved into a practical measurement tool in the 1990's [3] owing in part to the rapid advancement and widespread availability of inexpensive computational power. More recent applications of image correlation for measurements of high speed crack propagation and ballistic impact are discussed in references [4-5]. Some measurements of structural blast response, including aircraft structures, were described by the present authors in references [6-7]. The present work builds on the studies of [6-7] by providing new results for various types of explosives and structures.

2. DESCRIPTION OF THE IMAGE CORRELATION MEASUREMENT

Three dimensional image correlation uses stereo imaging of a patterned test surface in combination with pattern recognition and photogrammetry processes. This technology enables the quantitative full-field measurement of in-plane and out-of-plane displacement over the test surface in each photographic frame. It is only necessary that the surface pattern remain attached to the surface and the surface area

under study remain within the photographic view field throughout the test event. For more details about the digital image correlation measurement see references [6-7].

3. HIGH SPEED VIDEO SYSTEM

The basis of the image correlation system is a pair of Photron APX-RS monochrome video cameras. These cameras are capable of operation at frame rates up to 250,000 frames per second (fps), maximum resolution (at 3000 fps) of 1024 x 1024 pixels, and shutter speeds as high as 1 μ s. Each camera has 8 GB of internal memory. References [6-7] provide further details about the high speed video system.

4. MEASUREMENT ACCURACY CHARACTERISTICS

To establish the displacement measurement accuracy of the system a series of static displacement measurements was performed. A speckle patterned cast iron surface plate (254 mm wide x 356 mm tall, 13 μ m flatness) was used as the test surface. This plate was rigidly mounted to a rotary indexing table which allowed the test surface to be translated up to 200 mm either in its own plane or normal to itself, and rotated up to 360°. Error in the measured displacement in the out-of-plane direction was about 1% of the displacement for displacements greater than about 8 mm. This relative error magnitude changed little with frame rate between 3000 and 10,000 fps, camera angles in the range 20°-50°, and test surface obliqueness angles relative to the cameras in the range $\pm 40^\circ$. The effect of speckle pattern loss on accuracy was also modest, with relative errors in the measured displacement (in areas remote from the pattern loss) remaining below 1% for disc-shaped pattern-less areas of 20, 40, and 60 mm diameter. Further details of the accuracy validation testing are given in references [6-7].

5. BLAST RESPONSE OF PLATES, PANELS, AND AIRCRAFT STRUCTURES

Blast structural response has been measured using image correlation for three types of structures. These measurements are discussed below.

Blast response of a steel witness plate

It is necessary to evaluate the vulnerability of aircraft structures to damage by explosives of various types. To accomplish this evaluation process efficiently for a wide variety of explosives it is useful to implement the notion of explosive equivalence. This approach results in the assignment of the blast intensity (e.g. peak pressure or impulse) for the explosive under test relative to the intensity for a well-characterized reference explosive. It has been shown that under impulsive blast loading conditions the peak elastic deflection of a witness plate is proportional to the total impulse delivered to the plate by the blast. Although no single blast intensity characteristic is sufficient

to completely describe the equivalence relationship, blast impulse is probably the best single characteristic to use in the context of aircraft vulnerability. This is because the deflection and strain induced in a structure by an impulsive load correlates well with the magnitude of the impulse delivered to it. The elastic response of a circular steel witness plate to the detonation of bare explosive charges of several types was measured by image correlation in order to determine the explosive equivalence of these explosives in the sense of blast impulse.

The speckle patterned circular witness plate was 20.8 mm thick heat treated 4340 steel with tensile yield and ultimate stresses of 183 and 193 ksi, respectively. The 91.4 cm (36 in.) diameter witness plate was rigidly bolted over a 76.2 cm (30 in.) diameter hole in a 12.7 cm (5 in.) thick vertical steel bulkhead with 36 three-quarter inch Grade 8 steel bolts on an 83.8 cm (33 in.) bolt circle. Consult references [6-7] for further details about the witness plate test fixture. The steel alloy and thickness of the witness plate were chosen to yield an easily measurable but elastic response when subjected to the blast loads under study. The two high speed cameras were symmetrically located with respect to the witness plate center resulting in camera angles in the range 30-35° during the tests. Camera frame rate was 10,000 fps with corresponding 512 x 512 pixel image resolution. This frame rate corresponds to a 100 μ s interval between consecutive images.

The witness plate response for three different explosive charge types, differing in explosive compound and physical form, are discussed here. These charges will be referred to as charges α , β , and γ . The charge sizes are characterized by the charge weight. The charge weights are referenced in terms of a coded scale of weight measurement denoted here by the symbol C. The coded weights are proportional to the actual weights, however, the proportionality factor will not be revealed for security reasons. Similarly, the standoff distance of the charge from the witness plate center, held fixed throughout the testing, is withheld for security.

Witness Plate Deflection—A 3D contour-shape plot of the transverse witness plate deflection, measured by image correlation, is shown in Fig. 1 for a 16C weight of charge α . This deflection is measured relative to the pre-blast witness plate shape (flat with variations from planarity less than about 0.25 mm). The color contours in this plot are correlated to the deflection magnitude, denoted by the symbol W, in the legend appearing in Fig. 1. The X and Y coordinates in Fig. 1 are horizontal, increasing to the right, and vertical, increasing upward on the witness plate, respectively. The origin of the X and Y coordinates is at the plate center. The deformation shown in Fig. 1 corresponds to the peak deflection of the plate which occurs eight images or 800 μ s after the first image in which deformation is observed. The plate deformation is seen to be everywhere convex as viewed by the cameras and is approximately axisymmetric with respect to the plate center where the peak deflection is 7.95 mm. The plate deformed shape was found

to be similar, except for a deflection scaling factor, at other times during the response and for other weights of charge α . The greatest measured transverse velocity of the plate occurs at the center in the first 100-200 μ s of the deformation. The mean velocity of the plate center during this time interval is about 17.4 m/s. After this the plate velocity decreases dramatically. This early period of large plate velocity may correspond to the duration of the blast loading on the plate.

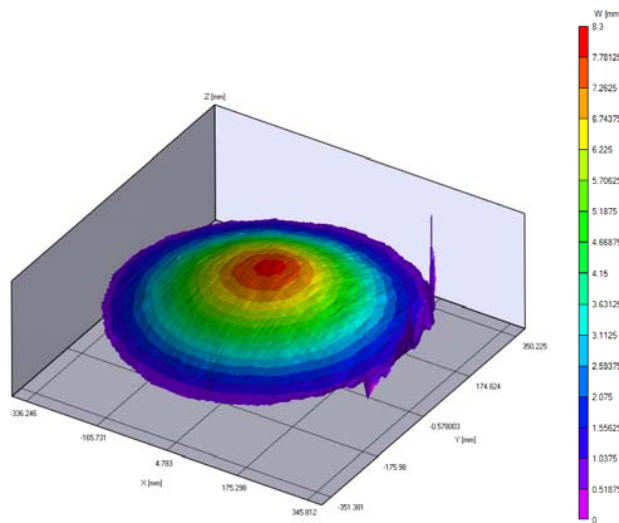


Figure 1. Contours of plate transverse displacement at peak deflection: Charge α , weight = 16C.

An axisymmetric deflection concavity of the witness plate was observed for charge types β and γ . The concave deformed shape is illustrated in Fig. 2 which shows normalized deflection profiles (normalized by the largest deflection on the plate) for tests with charges α and β plotted over the horizontal witness plate diameter. Note that the plate deformed shape at peak deflection is very similar for the two charge types except that the shape for charge α is slightly broader than for charge β . The pre-peak deflection profile for charge β reveals profile concavity over a circular region of about 200 mm diameter at the plate center. Charge γ also resulted in plate deformed shape concavity for a brief time during the first quarter oscillation period.

This distinct feature of the deformation observed for charges β and γ is probably an indication that the blast load on the witness plate for these charges has a different spatial and/or temporal distribution relative to the load imposed by α -type charges. The measurements also suggest that the load distribution for the β - and γ -type charges excites some higher axis-symmetric vibration modes in the plate which, conversely, are not excited by the loading due to the α -type charge.

Figure 3 shows the variation of witness plate peak deflection with charge weight for the three different explosive charges. The charge standoff from the witness plate was held fixed in

all tests shown in Fig. 3. The plotted data indicate that the peak deflection is most sensitive to charge size for charge type β and least sensitive for the α -type charges with the γ -type charges falling in between, cf. Fig. 3. It is also clear from Fig. 3 that for a given charge weight the type β charge results in measurably greater plate deflection than the γ charge and much greater deflection than the α charge. Charge types β and γ result in the same deflection as about 3 and 2.5 times the mass of charge α , respectively. Further, from the direct proportionality between plate peak deflection and blast impulse it follows that about 3 and 2.5 times the mass of charges β and γ , respectively, are required to deliver the same blast impulse to the witness plate using charges of type α .

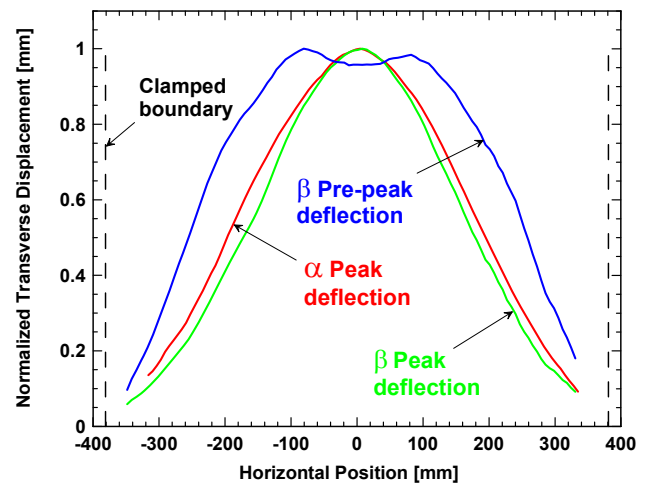


Figure 2. Normalized plate deflection profiles.

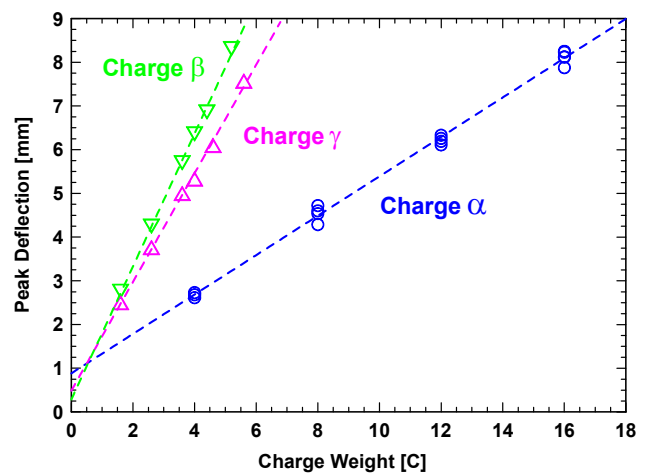


Figure 3. Plate peak deflection vs. charge weight.

Witness Plate Strain—Figure 4 shows the witness plate transverse deflection and principal strain histories at the plate center for tests with α - and β -type charges with weights 16C and 5.2C, respectively. The in-plane strain at the surface of the witness plate is calculated from the measured in-plane displacement field. Time zero in Fig. 4 coincides with the last undeformed image for each of the two tests shown. These charge weights yield very similar

peak plate deflection magnitudes (7.95 and 8.19 mm for α - and β -type charges, respectively) and therefore the magnitude of blast impulse delivered to the witness plate is also similar for these two charges. However, for the β charge the deflection increases non-monotonically during the first quarter-period of the plate oscillation owing to the brief period of deformation concavity which precedes the peak deflection.

Also, the two charge types display very different strain magnitudes and histories. Peak strain for the α -type charge, $\sim 2900 \mu\epsilon$, is achieved at approximately the same time as the peak transverse plate deflection. For the β charge the peak strain is much larger, $\sim 5100 \mu\epsilon$, and this peak strain is reached very early in the deformation process. Further, the strain is seen to be slightly compressive for a brief period at about 700 μs for the β charge due to the concave deformation shape existing at this time. Strain behavior for charge type γ was similar to the behavior shown in Fig. 4 for the β -type charge.

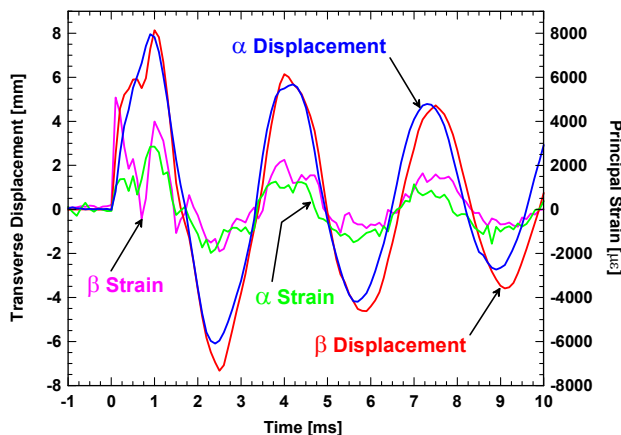


Figure 4. Time history of witness plate displacement and principal strain at plate center.

The measured witness plate deformation and strain response for the β - and γ -type charges is quite distinct from the response observed for the α charge type. Presumably the different responses result from commensurately disparate spatial and temporal blast loading characteristics for these charge types. Although explosive equivalence for the β and γ charges (relative to α) can be assigned on the basis of equal blast impulse delivered to the plate, this basis ignores the much higher strain which develops very abruptly in the plate for the β and γ charges. For the β and γ charges impulse delivery equivalent to the α charge does not imply equivalent strain or equivalent damage to the target structure. Therefore additional testing is warranted for these charges, perhaps using the stress or strain level directly, as the basis for equivalence assignment.

Blast-induced plastic deformation of an aluminum panel

Image correlation was used to measure the blast-induced response of a 1/8 inch thick 6061-T6 aluminum panel due to

detonation of a spherical charge of C-4 explosive. The panel was 122 cm (48 in.) square and was bolted over a 107 cm (42 in.) diameter circular hole in a massive vertical steel bulkhead. The panel was clamped to the steel bulkhead on the blast side of the bulkhead by a square steel backing frame which enveloped the 107 cm panel working diameter. Hence the freely deforming area of the square panel was circular but the panel was clamped over a square contour. The charge weight and the standoff distance between the charge and the panel center are here left unspecified for security reasons. Camera frame rate and image resolution were the same as in the measurements of witness plate deflection discussed above.

Panel Deflection—Figure 5 shows contours of the transverse deflection of the aluminum panel at peak deflection. The charge configuration is designated as charge configuration 1. This peak transverse deflection, of magnitude 125 mm, occurred at the panel center 21 images or 2.1 ms after the last photographic image without deformation. Therefore the average transverse velocity of the panel center from the initial undeformed condition to the peak deformation in Fig. 5 is about 60 m/s. The maximum velocity during the deformation process is actually far greater than this (see discussion below). The much larger velocities for the aluminum panel compared to the steel witness plate (~ 17 m/s), aside from variations in explosive type and standoff, are due to the much smaller mass of and different structural configuration of the aluminum panel.

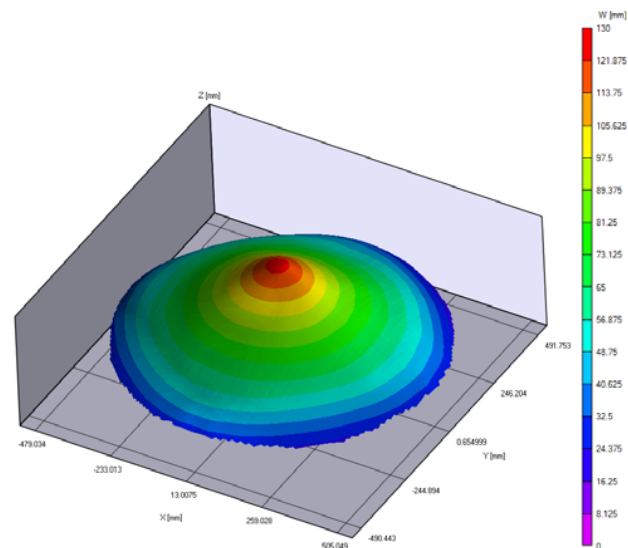


Figure 5. Contours of transverse deflection: 6061-T6 aluminum panel under charge configuration 1.

Figure 6 shows profiles of transverse deflection on the 6061 aluminum panel over the panel diameter $Y = 0$ at various times during the deformation process. These data correspond to a similar test with a charge configuration different from the test depicted in Fig. 5. It is designated as charge configuration 2. Time zero for the test in Fig. 6 corresponds to the last undeformed image. Note that the transverse velocity is greatest very early in the process.

Between the profiles corresponding to times 0.1 and 0.2 ms the average transverse velocity at the center of the panel is 300 m/s. This velocity is attained from rest in a time which is no greater than 200 μ s and is probably nearer to 100 μ s, therefore the mean acceleration of the panel center during this early deformation lies approximately between 150,000 and 300,000 g. The transverse velocity reduces rapidly as the peak deflection of 150 mm is approached at 2.2 ms. The profile shapes in Fig. 6 indicate strong curvature near the center of the panel within a radius of about 100 mm from the panel center. This curvature remains relatively constant from about 0.2 ms to the peak deflection at 2.2 ms. Although later profiles are not shown in Fig. 6 those later profiles, aside from some small elastic oscillation, indicate very nearly the same shape and deflection magnitude shown in Fig. 6 at peak deflection. The absence of significant deflection rebound suggests that most of the panel deformation observed in the peak deflection profile is due to plastic strain.

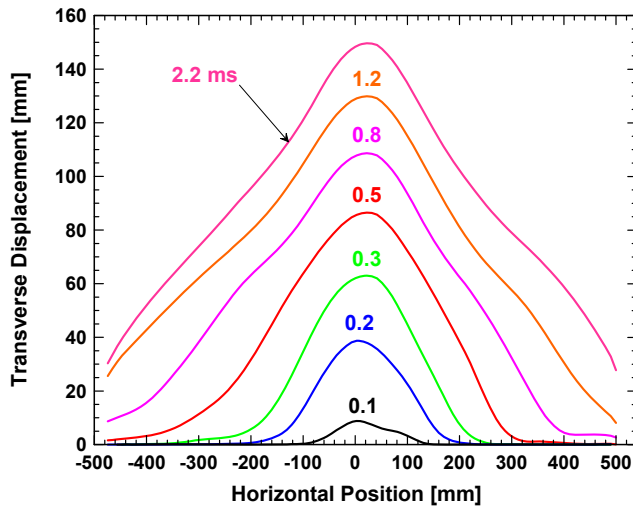


Figure 6. Deflection profiles: 6061-T6 panel under charge configuration 2.

Panel Strain—Figure 7 shows the time histories of the transverse displacement and the first principal strain at the center of the aluminum panel corresponding to the deflection profiles plotted in Fig. 6. The symbols correspond to individual image correlation measurements of deflection and strain at the panel center in each image. Except for some damped oscillations the deflection magnitude changes relatively little after the peak deflection of 150 mm is reached at about 2.2 ms. The deflection history in Fig. 7 supports the conclusion reached on the basis of the deflection profiles in Fig. 6 that most of the initial deformation is plastic deformation. This conclusion is further supported by the strain history at the panel center, also plotted in Fig. 7. Close examination of the strain variation in Fig. 7 indicates that the peak strain at the panel center is achieved only about 3 images or 300 μ s after the first deformed image. After this time the strain is relatively constant at about 0.086 or 8.6%. Since this strain magnitude is far in excess of the yield strain of about 4000 μ e (0.4%)

for this 6061 alloy, the material at the center of the panel has clearly experienced large plastic deformation. This strain level, however, is well below the 17% elongation at rupture measured in quasi-static testing for 6061-T6 aluminum [8].

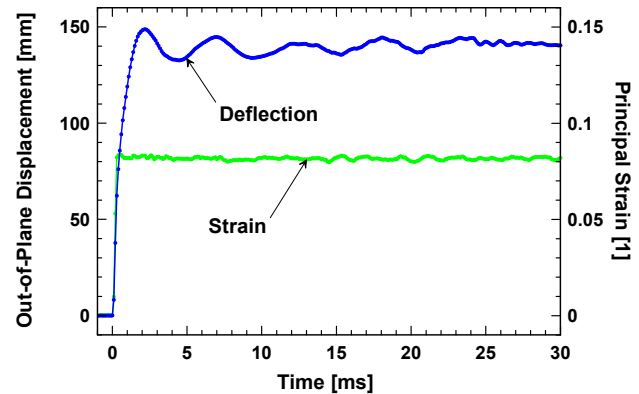


Figure 7. Deflection and strain history at center: 6061-T6 panel under charge configuration 2.

Blast response of commercial aircraft fuselage skin

Image correlation measurements were made on the external skin of a pressurized commercial aircraft during an internal blast test. In this test a portion of the cargo hold was protected by a flexible panel of blast mitigation material which was attached to the inboard side of the airframe. The blast was due to a spherical explosive charge which was placed inside a suitcase filled with typical luggage contents. The suitcase was located in the cargo hold adjacent to the mitigation panel at a particular distance, to remain unspecified here, from the inboard surface of the mitigation panel. During the course of this test the aircraft skin experienced significant radial deflection and modest permanent deformation in the neighborhood of the charge location, but it did not rupture. Because the skin failed completely in a similar test without a blast mitigation panel and without pressurization survival of the skin in the present test is attributed to the presence of the panel. The image correlation data presented below reveal the basic mechanisms by which the mitigation panel allows the aircraft structure to survive the blast loading.

The blast mitigation panel spanned a rectangular section of the fuselage skin in the cargo bay encompassing three frame bays in the longitudinal direction and six stringers in the circumferential direction. The panel was screwed into longitudinal intercostal structures which extended radially outward from the plane of the mitigation panel to the stringers in between the frames. These intercostals were riveted to the stringers at the outboard edge thus providing robust mechanical coupling between the mitigation panel and the stringers which are in direct contact with the aircraft skin.

The external skin of the aircraft was speckle painted over the cargo bay area protected by the blast mitigation panel. The two high speed video cameras were focused on this section of the external skin, about 3 m (9.8 ft) from the skin

and separated by approximately 2 m (6.6 ft). Photographic images of the blast-induced skin deformation were recorded using a frame rate of 9,000 fps and an image resolution of 640 x 480 pixels. This frame rate corresponds to 111 μ s spacing between consecutive photographic images. Artificial and natural illumination of the test surface allowed a shutter speed of 25 μ s. For image correlation analysis deformation of the skin is measured with respect to a cylindrical coordinate system which is fitted to the undeformed skin surface by the image correlation software. The radial, axial (longitudinal), and circumferential displacements of the skin are measured in this cylindrical coordinate system with respect to the position of the skin in the undeformed (aside from deformation due to internal pressurization) pre-blast condition. Because of precise camera triggering and timing the elapsed time between detonation and each photographic image is known. In the analysis and discussion presented below all times are measured relative to charge detonation (time = zero) which occurred in image 35. Note that image correlation-derived skin deflection and strain are indicative of blast deformation only and do not include the deformation due to pre-blast fuselage pressurization.

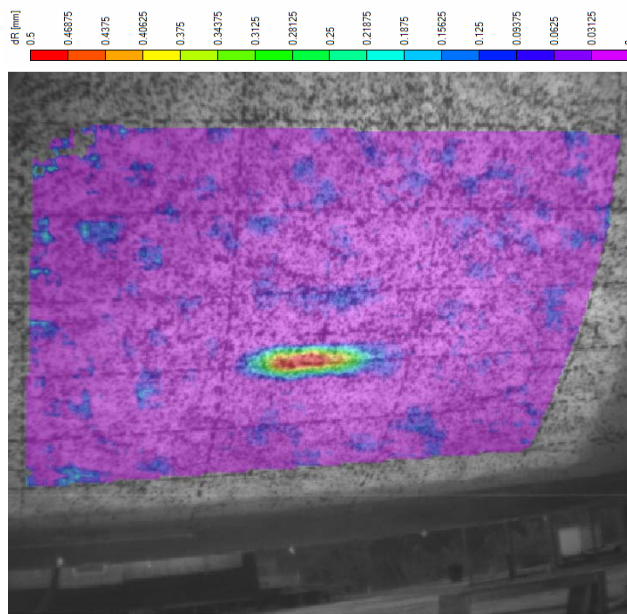


Figure 8. Radial deflection contours: Image 38 (0.33 ms).

Radial Skin Deflection—The first image showing measurable radial deflection of the skin was image 38. This image follows charge detonation by three images or 333 μ s. Color contours of the radial skin deflection (relative to the pre-blast condition) measured by image correlation are superimposed onto image 38 and plotted in Fig. 8. The approximate frame and stringer positions can be seen in Fig. 8 as vertical and horizontal dashed lines, respectively, drawn on the fuselage skin. The charge location is shown as a cross on the skin near the center of the image and midway between the center pairs of frames and stringers. For reference, the forward direction on the aircraft is to the left

in this figure. The correlation between the contour colors and radial skin displacement, denoted as dR , is given in the legend above the plot in Fig. 8. The deflection contours are displayed using sixteen equal deflection intervals ranging from 0 to 0.5 mm. Note that radial displacement of the skin in image 38 is confined principally to the stringer just below the charge location. The peak radial displacement at this stringer is ~ 0.6 mm. Radial displacement at the stringer just above the charge location, barely detectable in Fig. 8, is less than 100 μ m. No skin deformation has occurred at the charge location or at the frames adjacent to the charge in image 38.

Radial skin displacement contours for image 44, corresponding to one millisecond after detonation, are shown in Fig. 9. At this time the skin deformation encompasses the entire skin area within the charge bay (i.e., the bay bounded by the frame and stringer pairs immediately adjacent to the charge location). The greatest displacement, 12 mm, is now found at the center of the upper stringer bounding the charge bay, almost directly above the charge location. Further, the deflection contour shapes in the immediate neighborhood of the charge bay suggest that in addition to the stringers the frames are now also transmitting some modest (relative to the stringers) amount of blast load to the skin. In subsequent images the skin deformation process is seen to spread beyond the charge bay into the adjacent bays above and below and forward and aft of the charge bay. With time the deformation becomes more uniformly distributed and eventually spreads outward from the frame bay to the limits of the imaged skin section while increasing in magnitude at the same time. The peak radial skin deflection measured in the test occurs in image 74 at 4.33 ms after detonation. The peak radial deflection of 38.1 mm occurs at the forward end of the charge bay.

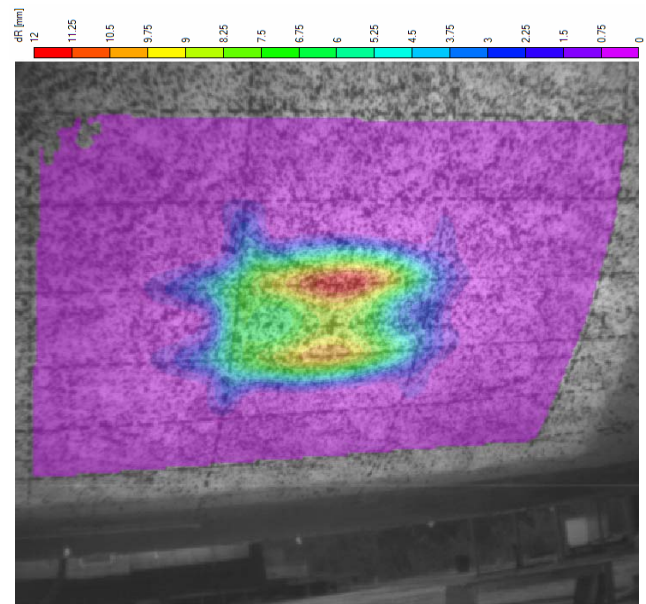


Figure 9. Radial deflection contours: Image 44 (1.00 ms).

Figure 10 shows profiles of radial skin deflection plotted over a circumferential contour on the skin (parallel to the frames) and passing through the charge location. Profiles are included for ten different times ranging from 0.44 ms (image 39) to 4.3 ms (image 74, peak deflection). Also sketched as horizontal dashed lines on the plot in Fig. 10, for reference, are the approximate positions of the stringers adjacent to the charge. These stringers are located approximately 100 mm above and below the charge location which corresponds to the origin on the vertical axis in Fig. 10. The well-defined deformation in the neighborhood of these stringers early in the process is consistent with highly efficient mechanical coupling of the blast forces to the skin via the intercostal structures which effectively bridge the space between the mitigation panel and the stringers.

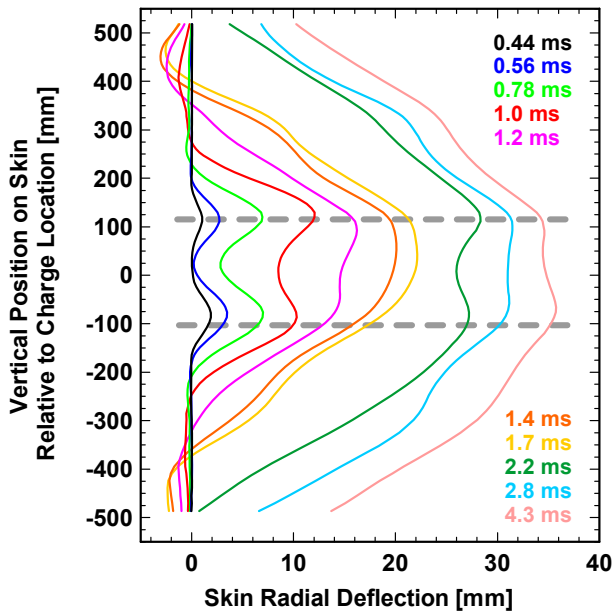


Figure 10. Radial skin deflection profiles on a circumferential contour through the charge location.

For profiles corresponding to times greater than about 1.4 ms after detonation there is also evidence that the next stringer pair, above and below the charge bay, are transmitting modest load to the skin. These stringers are located, very approximately, 300 mm above and below the charge location. Measurements of the radial skin deflection have demonstrated that the mitigation panel and airframe system causes the blast load to be distributed over a large portion of the aircraft skin in a controlled manner instead of allowing a highly impulsive and spatially concentrated load to act over a relatively small area of the skin, as would occur in the absence of mitigation.

Skin Strain—The strain in the skin, calculated from the in-plane displacement field, is greatest early in the process in the neighborhood of the stringers which straddle the charge position. The strain mirrors the early radial skin deflection which is concentrated along these stringers.

Figure 11 shows contours of the first principal strain for image 66, 3.44 ms after detonation. The largest strain observed for the entire test is measured in this image. This strain, of magnitude 16,000 $\mu\epsilon$ or 1.6%, occurs in the bay above the charge bay just slightly aft of the frame which is immediately forward of the charge location. The second largest strain in this image, $\sim 1.4\%$, is observed in a symmetrical position with respect to a circumferential line through the charge location, near the frame which is immediately aft of the charge. Figure 11 indicates that strain levels in the bay above the charge bay are considerably larger than those in any other bay, including the charge bay. The strain level in this bay is mostly in the range 0.5-1.6% which exceeds the yield strain of 0.45-0.50% for the 2024-T3 skin alloy. This indicates that most of the skin in this bay has experienced some plastic deformation. The strains within the charge bay, on the other hand, are mostly below 0.5% indicating mostly elastic strain there. Currently, no satisfactory explanation has been found for the appearance of these plastic strains in the bay above the charge bay.

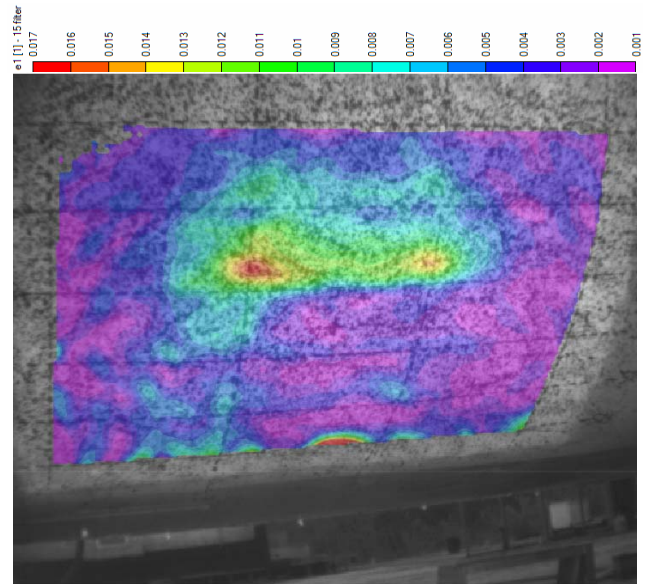


Figure 11. Contours of first principal strain: Image 66 (3.44 ms).

Figure 12 shows the time history of the radial skin deflection and principal strain at the position of maximum strain observed in Fig. 11. The strain peak of 1.6% occurs about 700 μs before the deflection peak of ~ 33 mm. Note that the strain remains at the 0.9-1% level well after the radial deflection at this position has diminished to zero. This is consistent with the existence of residual plastic strain in the skin at this location. Although the skin at this position and throughout most of the bay above the charge bay has experienced considerable plastic deformation the measured strain is still far below the 18% elongation at failure for the 2024-T3 skin alloy.

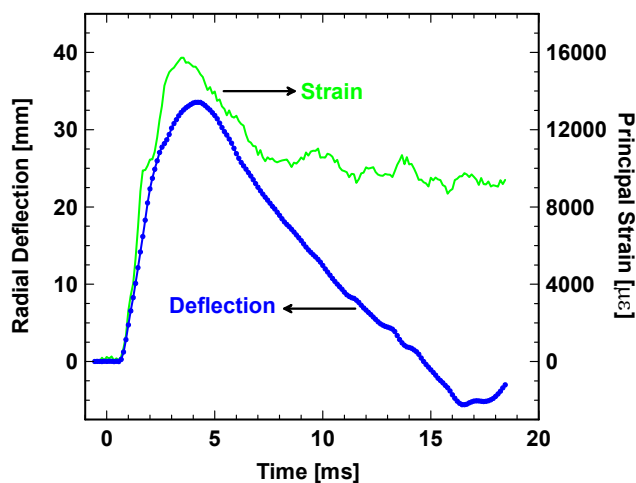


Figure 12. Radial skin deflection and strain history at location of maximum strain.

6. CONCLUSIONS

Digital image correlation has been used to make full-field non-contact measurements of the blast-induced response of three different structures. These structures included a steel witness plate, a thin aluminum alloy panel, and the cargo bay area of a pressurized commercial aircraft fuselage which was protected by a blast mitigation panel. This measurement approach made it possible to study the time evolution of the deforming shape of these structural surfaces as well as the spatial distributions and time histories of transverse deflection and strain. Measurements of witness plate peak deflection facilitated the determination of relative explosive equivalence for three different charge types in the sense of blast impulse. Measurements of witness plate strain suggested that blast impulse alone may not be sufficient to fully characterize blast potency and structural damage for some of the charge types tested. Correlation measurements for the blast response of a thin aluminum panel indicated a peak transverse deflection of 150 mm, panel velocity of 300 m/s, acceleration from 150,000 to 300,000 g, and large plastic strain in the blast-affected area exceeding 8%. Measurements of the skin deformation for an internal blast in the cargo bay of a pressurized aircraft revealed the physical mechanisms which permitted a blast mitigation panel to prevent skin breach. Rather than allowing a highly impulsive and spatially concentrated load to act over a relatively small area of the skin, correlation measurements showed that the mitigation panel caused the blast load to be distributed over a sizable portion of the frame and stringer system. These results demonstrate that image correlation is an important technique for gathering critical structural response data during blast testing which may be too severe or hazardous for other measurement approaches.

7. REFERENCES

[1] Sutton, M. A., Wolters, W. J., Peters, W. H., Ranson, W. F., McNeil, S. R., "Determination of Displacements Using an Improved Digital Correlation Method," *Image and Vision Computing*, 1983, Vol. 1, No. 3, pp. 133-139.

[2] Bruck, H. A., McNeil, S. R., Sutton, M. A., Peters, W. H., "Digital Image Correlation Using Newton-Raphson Method of Partial Differential Correction" *Experimental Mechanics*, 1989, Vol. 28, pp. 261-267.

[3] McNeil, S. R., Sutton, M. A., Miao, Z., Ma, J., "Measurement of Surface Profiles Using Digital Image Correlation," *Experimental Mechanics*, 1997, Vol. 37, No. 1, pp. 13-20.

[4] McNeil, S. R., Sutton, M. A., Chao, Y. J., Bruck, H. A., "Characterization of Impact Damage Evolution in Functionally Graded Composites Using Novel Nanosecond 3D Deformation Measurement System," *16th US Army Symposium on Solid Mechanics*, Charleston, SC, May 2003.

[5] Kirugulige, M. S., Tippur, H. V., Denney, T. S., "Measurement of Transient Deformations Using Digital Image Correlation Method and High Speed Photography," *Applied Optics*, 2007, Vol. 46, pp. 5083-5096.

[6] Nansteel, M. W. and Chen, C., "High Speed Photography and Image Correlation for Studying the Blast Response of Aircraft Structures," *78th SAVIAC Shock and Vibration Symposium*, November 4-8, 2007, Philadelphia, PA.

[7] Nansteel, M. W. and Chen, C., "High Speed Photography and Digital Image Correlation for the Study of Blast Structural Response," *ITEA Journal*, to appear 2009.

[8] Lynch, C.T. *Practical Handbook of Materials Science*, CRC Press, 1989.